Article:
He, X. orcid.org/0000-0002-2214-9338, Jiang, X. orcid.org/0000-0003-4141-1538, Spracklen, D.V. orcid.org/0000-0002-7551-4597 et al. (8 more authors) (2023) Global distribution and climatic controls of natural mountain treelines. Global Change Biology. ISSN 1354-1013

https://doi.org/10.1111/gcb.16885

Global distribution and climatic controls of natural mountain treelines

Running title: Climate treeline patterns and drivers

Xinyue He[1,2], Xin Jiang[1], Dominick V. Spracklen[2], Joseph Holden[3], Eryuan Liang[4,5], Hongyan Liu[6], Chongyang Xu[6], Jianhui Du[7], Kai Zhu[8,9], Paul R. Elsen[10], Zhenzhong Zeng[1*]

[1] School of Environmental Science and Engineering, Southern University of Science and Technology, Shenzhen, China

[2] School of Earth and Environment, University of Leeds, Leeds, UK

[3] School of Geography, University of Leeds, Leeds, UK

[4] Key Laboratory of Alpine Ecology, Institute of Tibetan Plateau Research, Chinese Academy of Sciences, Beijing, China

[5] CAS Center for Excellence in Tibetan Plateau Earth Sciences, Beijing, China

[6] College of Urban and Environmental Science and MOE Laboratory for Earth Surface Processes, Peking University, Beijing, China

[7] School of Geography and Planning, Sun Yat-Sen University, Guangzhou, 510275, China

[8] Department of Environmental Studies, University of California, Santa Cruz, California, USA

[9] Institute for Global Change Biology and School for Environment and Sustainability, University of Michigan, Ann Arbor, MI 48109, United States

[10] Wildlife Conservation Society, Global Conservation Program, Bronx, NY, USA

*Correspondence to: zengzz@sustech.edu.cn (Z. Zeng)

Abstract

Mountain treelines are thought to be sensitive to climate change. However, how climate impacts mountain treelines is not yet fully understood as treelines may also be affected by other human activities. Here we focus on "closed-loop" mountain treelines (CLMT) that completely encircle a mountain and are less likely to have been influenced by human land-use change. We detect a total length of ~916,425 km of CLMT across 243 mountain ranges globally and reveal a bimodal latitudinal distribution of treeline elevations with higher treeline elevations occurring at greater distances from the coast. Spatially, we find that temperature is the main climatic driver of treeline elevation in boreal and tropical regions, whereas precipitation drives CLMT position in temperate zones. Temporally, we show that 70% of CLMT have moved upwards, with a mean shift rate of 1.2 m/year over the first decade of the 21st century. CLMT are shifting fastest in the tropics (mean of 3.1 m/year), but with greater variability. Our work provides a new mountain treeline database that isolates climate impacts from other anthropogenic pressures, and has important implications for biodiversity, natural resources, and ecosystem adaptation in a changing climate.

Keywords: treeline, forest boundary, tree cover, climate, mountain ecosystems, alpine area

1. Introduction

The mountain treeline is the upper altitudinal limit of tree growth toward the top of mountains, a transitional zone from forests to treeless alpine vegetation (Körner & Paulsen, 2004). Treeline ecotones play important environmental roles, including as habitats for endemic species and by contributing to water supply (Grace, 1989). Mountain treelines are important indicators of the impact of climate change on upland ecosystems (Verrall & Pickering, 2020; Lu et al., 2021) as they are strongly associated with growing season lengths and minimum daily temperatures (Paulsen & Körner 2014). Consequently, as a response to global warming, mountain treelines are expected to shift upward as high elevations become more favourable for tree establishment under a changing climate (Holtmeier & Broll, 2005; Du et al., 2018). Furthermore, treeline shifts give rise to novel high-elevation vegetation patterns and could redefine habitable area for forest-dependent species in a warmer future world (Bolton et al., 2018; Mohapatra et al., 2019). However, the treelines in many mountain regions have been heavily altered by land-use change and land-use management (Gehrig-Fasel et al., 2007; Ameztegui et al., 2016). Such land-use driven treelines are generally lower than the elevation of the local theoretical climatic treelines, making it difficult to isolate potential influences of climate on treeline position and obscuring the impact of climate change on treeline shifts. Therefore, accurate and reproducible detection of natural mountain treelines and their shifts are of great importance to understanding global climate change and the associated response of vegetation dynamics in alpine areas in natural systems.

Previous studies reporting local treeline sites have mainly relied on field investigation (Wardle & Coleman, 1992; Liang et al., 2014; Elliott & Cowell, 2015; Sigdel et al., 2018). While such studies have enhanced our understanding of treeline patterns, a key limitation of field-based studies is sparse geographic coverage. Remote sensing can overcome such a limitation by providing globally consistent coverage, but the determination of treeline positions only through visually interpreting satellite imagery (Paulsen & Körner, 2014; Irl et al., 2016; Karger et al., 2019) is time-consuming

and labour-intensive at large spatial scales. Recently, regional attempts to combine remote sensing data with automated image processing techniques have emerged (Wei et al., 2020; Xu et al., 2020; Wang et al., 2022; Birre et al., 2023), but inconsistent analytical approaches and treeline definitions complicate regional comparisons and make it difficult to generalize global patterns. Early assessment at the global scale suggested that low temperatures limited tree growth at treelines (Körner & Paulsen, 2004), but there is also regional evidence that tree growth at the treeline does not increase under global warming due to moisture limitations (Liang et al., 2014; Lyu et al., 2019; Camarero et al., 2021). A generalizable pattern of the climatic limiting factors of global treelines is still lacking.

The aforementioned challenges and limitations associated with delineating treelines and determining climatic influences on treeline positions have hindered our understanding of the global impact of climate on treelines in natural systems. To address this issue, we focused on "closed-loop" mountain treelines (CLMT)—treelines with a continuous band of tree cover around a mountain. Such systems are less likely to have been influenced by land-use change. By focusing on this subset of treelines, we are better able to exclude treelines that may be impacted by topographic constraints or anthropogenic land use in order to isolate the effects of climate on mountain treelines in natural systems. An advance over previous studies that only provide a handful of data points for each treeline is a complete depiction of treeline at 30 m resolution. Our approach allows us to calculate the treeline elevation around the entire treeline, providing unprecedented detail on the variability of treeline elevation at the local scale. More importantly, using CLMT as a proxy for natural treelines with little influence from land-use change allows us to make a new and more robust assessment of how natural treelines are responding to changes in climate.

Here, we map closed-loop treelines in mountain regions globally in 2000 based on remote sensing, via integrating a high-resolution tree cover map (Hansen et al., 2013) with a digital elevation model

at the same spatial resolution (Tachikawa et al., 2011). For this purpose, we develop a novel automatic detection algorithm that can produce consistent characterizations of CLMT across space. Our detection of mountain treeline is based on tree cover data that consider trees as any vegetation taller than 5 m (Hansen et al., 2013), using a 5% tree cover threshold to delineate forested and non-forested areas. The algorithm starts from the highest elevation point for each mountain range and generates a forest boundary map from which we extract the closed-loop treelines. To further ensure that our CLMT are natural treelines that are not impacted by anthropogenic disturbances, we conduct a manual inspection of high-resolution imagery to remove treelines with any indication of anthropogenic land use and restrict our analysis to regions where the human footprint is low (Mu et al., 2022). To understand which bioclimatic factors control the position of natural mountain treelines from global to local scales, we use the gradient boosting decision trees (GBDT) model (Friedman, 2001) to calculate the feature importance of each temperature or precipitation variable. Further, we map the new natural treeline positions in 2010 using the same algorithm above and the amount of tree cover in 2010 (Hansen et al., 2013) to explore the shifting of mountain treelines in natural systems.

2. Methods

2.1. Tree canopy cover data

We used a high-resolution remote sensing global map of tree canopy cover for the year 2000 (Hansen et al., 2013) to delineate forested and non-forested areas. The dataset was produced at a 30 m resolution based on multiple types of forest sample data and spectral curves of Landsat time series using a decision tree method (Hansen et al., 2013). To test which tree cover threshold is suitable for treeline mapping, we undertook a sensitivity analysis with different thresholds in mountains, finding there is little difference among different thresholds from 0 to 10% (examples refer to Figs. S1–S3). Thus, we took the mean value of 0 to 10%, namely 5%, as the tree cover threshold, and define the treeline to be the transition zone above which tree cover is ≤5% and below

which tree cover is >5%. We then binary-classified the tree canopy cover data using the threshold, assigning a value of 1 for the alpine land zone (the area above treeline) with tree cover ≤5% (non-forested area), and 0 for pixels with greater than 5% tree cover (forested area).

2.2. Topography data

We combined global mountain polygons with a high-resolution digital elevation model to restrict the search area of mountain treelines. Mountain boundaries were collected from the Global Mountain Biodiversity Assessment (GMBA) inventory (version 1.2; Körner et al., 2017). The GMBA inventory delineated global mountains into discrete regions (polygons) based on topographic ruggedness metrics and expert delineation (Körner et al., 2017). The elevation information in mountains was provided by the Advanced Spaceborne Thermal Emission and Reflection Radiometer Global Digital Elevation Model (version 3; Tachikawa et al., 2011) at a spatial resolution of 30 m.

2.3. Iterative mountain treeline extraction algorithm

We developed an algorithm to automatically detect CLMT (Fig. S4). We first determined the coordinates of the highest peak within each mountain region. The algorithm starts at this peak point if it is within the alpine area that is non-forested, then expands outward (i.e., downslope), and determines all other pixels of the image that are connected to the point and equivalent (marked as "1"). The eight neighbourhood region of the pixel $I(x, y)$ is expressed as:

$$R8 = \{(x + i, y + j); i, j \in (-1,1)\} \quad (1)$$

where *I, j* are integers. In the collection of the eight neighbourhood pixels, if $I(x, y) = I(x + i, y + j)$, there are connected relationships. The connected domain generated by this method is the connected alpine area. Because the algorithm determines the starting search point, we marked only one connected domain (namely the treeline zone) after one iteration.

To accelerate the efficiency of the algorithm, we set search blocks to determine the full altitudinal range of treelines within mountain ranges (Fig. S4). Specifically, the first round of the search takes the highest point of the mountain as the centre and the buffer zone with a side length of R as the search area for the treeline. After testing, the square area with 8,000 rows/ranks (side length R about 240 km) covered most alpine areas of mountains. For some of the mountaintops larger than this range, we expanded the side length to ~720 km to ensure that all close-loop mountain treelines of the world's mountaintops were covered.

There may be multiple treelines within a mountain range because a mountain may have multiple peaks. To account for this, we next searched for the second highest starting point (i.e., the highest point of the unsearched part) and repeated the process until the selected highest point was covered by forests (tree cover >5%).

After each iteration, the loops that were determined to be "open" were removed. Focusing only on closed treeline loops generated from the algorithm, we then visually inspected all loops using Google Earth (with spatial resolution ranging from 15 m to ~15 cm) to further exclude treelines with apparent signs of anthropogenic disturbances, such as roads, buildings, or croplands and removed the part of water bodies (i.e., pixels that were determined to be water). Last, we filled all the holes in the closed-loop polygons using the "imfill" function and extracted the edges of the binary images using the "bwperim" function in Matlab R2019a to obtain the CLMT positions.

To validate the robustness of the elevational distribution of CLMT derived from satellite images, at the pixel level, we used an independent validation dataset by manual interpretation using Google Earth's high-resolution images. We randomly produced 100 validation samples at a spatial resolution of 30 m. On a larger scale, we validated our CLMT database by comparison with *in situ*

168 measures (n = 62; Table S1). For each treeline site, we corresponded it to the closest treeline loop
169 detected in this study and compared its elevation with the range of the corresponding treeline loop.
170
171 **2.4. Climate data**
172 Considering the effect of climatic lag effects on treelines (Harsch et al., 2009), we used the climate
173 data from WorldClim (version 2.1; Fick and Hijmans, 2017), which provided the average for the
174 years 1970–2000 at a resolution of 30 seconds (~1 km^2), to understand which climate variables are
175 important in controlling treeline elevations. We used bioclimatic variables, which were derived
176 from monthly temperature and precipitation. A total of eight temperature variables and eight
177 precipitation variables were included, representing annual trends, seasonality, and extreme or
178 limiting environmental factors. They are annual mean temperature (annual T), temperature
179 seasonality (T seasonality; calculated as the standard deviation of the monthly mean temperatures,
180 then multiply by 100), the maximum temperature of the warmest month (maximum T), the
181 minimum temperature of the coldest month (minimum T), mean temperature of the wettest quarter
182 (wet season T), mean temperature of the driest quarter (dry season T), mean temperature of the
183 warmest quarter (warm season T), mean temperature of the coldest quarter (cold season T), annual
184 precipitation (annual P), precipitation of the wettest month (maximum P), precipitation of the driest
185 month (minimum P), precipitation seasonality (P seasonality; calculated as the coefficient of
186 variation, which is the ratio of the standard deviation to the mean), precipitation of the wettest
187 quarter (wet season P), precipitation of the driest quarter (dry season P), precipitation of the
188 warmest quarter (warm season P), and precipitation of the coldest quarter (cold season P). A
189 'quarter' here refers to any consecutive three months. For example, the coldest quarter consists of
190 the three months that are colder than any other set of three consecutive months. For each pixel
191 determined to be on a CLMT, we extracted the values of all 16 climate variables.
192
193 **2.5. Gradient boosting decision trees (GBDT) model**

We applied a GBDT method to model the treeline elevation as a function of climate factors. The GBDT model is a type of tree model with good interpretability for feature values (Friedman, 2001), which assembles and iterates over multiple regression trees, with the values of the negative gradient of the loss function in the model as an approximation of the residuals of the lifting tree algorithm in the regression problem (Ke et al., 2017). It is flexible in handling large amounts of data and often performs well in dealing with complex relationships in data (Ke et al., 2017). The GBDT initializes a weak learner, estimating a constant value of the loss of function minimization, and then creates decision trees according to the datasets and performs iterative training on them. Next, it calculates the negative gradient for loss of function (residuals) corresponding to each tree, fits a regression tree to the residuals to obtain the leaf node region of the m-th tree, and minimizes loss of function by estimating the values of all leaf node regions using a linear search. Last, GBDT repeats the above steps until the target evaluation indicator is optimal. Using this model, we calculated the feature importance of each variable and determined the dependent correlations for each factor after the model was built. The GBDT analysis was undertaken in Python 3.7 with the "sklearn.ensemble" module.

We carried out the GBDT analyses at global and local scales, as well as separately for different climatic belts (i.e., boreal, temperate, and tropical regions). At the global and regional scales, we considered each treeline loop as a sample, namely, using the mean of treeline elevation in each loop for the analysis. A total of 1,690 samples (treeline loops) were used for the global model. At the local scale, we regarded one treeline pixel as a sample. Hence, in each treeline loop, the repeated GBDT model represents the local effect of climate factors on treeline positions.

2.6. Mountain treeline shift rate

We mapped the new treeline positions in 2010 based on the global 2010 tree cover data (Hansen et al., 2013; Potapov et al., 2015), which is an update of the 2000 tree cover product. Using this dataset,

we re-ran the algorithm around treelines to detect the new closed-loop treelines in 2010. Starting from the highest elevation point we detected before, we expanded the rectangular area of the original treeline around by 10 km as the search area. Then we manually checked the results from the 1,690 treeline loops to (i) exclude treelines without closed loops; (ii) isolate examples of "broken treeline loops" and restrict them to corresponding areas in 2000 and 2010 (Fig. S5); and (iii) remove outliers (>95th percentile of both increasing and decreasing rates) to avoid the inclusion of any special cases with extremely steep changes. This filtering resulted in 1,110 treeline loops in 2010 (65.7% of all treelines initially assessed) being available for analysis of the treeline change. The main reason for the reduction in number of treeline loops between 2000 and 2010 is that some of the closed-loop treelines detected in 2000 did not form closed loops in 2010. We then calculated the mean elevation of closed-loop treelines in 2010 and the corresponding treelines in 2000 and used the difference to represent the treeline change over the 10-year period. The treeline shift rate (m/year) at each treeline loop was calculated as follows:

$$shift\ rate = \frac{\text{mean elevation 2010} - \text{mean elevation 2000}}{\text{10 yrs}} \quad (2)$$

3. Results

3.1. A map of global closed-loop mountain treelines

We detected 27,468,662 closed-loop mountain treeline positions (pixels at 30 m resolution) across 243 mountain ranges globally. The total length of CLMT we detected is ~916,425 km. Those treeline pixels form 1,690 treeline loops covering all continents except Antarctica, ranging from 64°N (Khrebet Polyarnyy, Russia) to 46°S (Princess Mountains, New Zealand), with mean elevations spanning from 489 ±283 m on Khrebet Chayatyn (Russia) to 4,528 ±104 m on Ruwenzori (Uganda, Kenya). The average length of these treeline loops is 542 km, and the average alpine land area above them is 142 km^2. To visualize global patterns of the elevation of CLMT, we calculated the mean elevation for each treeline loop and plotted their locations using the mean latitude and longitude of treeline pixels at 30 m resolution in each loop (Fig. 1a). The CLMT

derived from satellite tree cover data are consistent with fine resolution remote sensing images available on Google Earth (Fig. 1b-g). At the pixel level, the CLMT showed good agreement with manually interpreted data at 30 m resolution (R^2 = 0.96; Fig. S6). On a larger scale, the validity of our CLMT database was further supported by corroboration against *in situ* measures from previous studies (n = 62 measurements; Table S1), which fall within the elevation range of treeline loops (R^2 = 0.98; Fig. S7).

We found a bimodal pattern for the closed-loop mountain treeline elevation along latitude, with peaks at the equator and ~25°N (Fig. 2a). Between 0° and 10°, the elevation of CLMT is symmetrical in the northern and southern hemispheres, but beyond this range, treeline elevations in the northern hemisphere are higher than those in the southern hemisphere at equivalent latitudes (Fig. 2a), which is attributed to the oceanic influence on a smaller southern landmass (Cieraad et al., 2014). Our global CLMT distribution is consistent with previous global assessments, though there are some differences. In the tropics, the elevation of CLMT reaches up to 3,500 m (Fig. 2), a lower elevation than in a recent global assessment by Testolin et al. (2020) that reported tropical treelines higher than 4000 m. This discrepancy may be due to our strict definition of trees, >5 m height, as well as the exclusion of some unilateral and non-closed treelines in high mountains. At low latitude (especially at 0-20°N), there is large variation in the range of CLMT elevation (Fig. 2a). Among different continents, South America has a large CLMT elevation range variation. At 50°N–60°N and 20°N–30°N, many mountains in Asia and North America have similar treeline elevations, whereas there is a rather different behaviour at 30°N–50°N where treelines in North America are higher than those in Europe and Asia (Fig. 2a). To help understand what causes this behaviour, we calculated the distance to the coast for each treeline. We found lower treelines in coastal mountains at the same latitude (Fig. 2a) as has been suggested in the literature (Irl et al., 2016), which can be largely attributed to the thermo-dynamic effect of large high-elevation landmasses (Karger et al., 2019). At 30°N–60°N, mountains close to the coast have lower treelines

than their latitude might suggest (i.e., fall below the fitted curve; Fig. 2a). Similarly, along with longitude decreasing from 150°W to 100°W, treeline elevations in North America increase due to an increase in the distance to the coast (Fig. 2b).

3.2. Climatic determinants of closed-loop mountain treelines

We found that T seasonality, cold season P, and warm season T predict nearly 60% of the spatial distribution of CLMT globally (Fig. 3a). We then assessed how the three leading factors modulated the elevation of CLMT spatially. The results showed the abrupt transition of CLMT elevation occurring at the T seasonality threshold of ~9°C, but attenuated transitions in areas where T seasonality exceeded 10°C (Fig. S8a). Similarly, there is a CLMT elevation gradient that is spatially driven by cold season P, with abrupt transitions occurring at the thresholds of 320 mm and 450 mm along the gradient of cold season P (Fig. S8b). By contrast, we did not find such a dramatic transition of CLMT elevation along the warm season T gradient (Fig. S8c).

Collectively, temperature-related factors (64%) are more important than precipitation-related factors for limiting CLMT elevations on a global scale (Fig. 3a). In different latitudinal belts, temperature-related factors are most important in boreal and tropical regions, especially the temperature of the warmest and the wettest quarters, respectively, while precipitation dominates the CLMT elevation in temperate regions (Fig. 3b,c,d). We found that T seasonality is the most important individual factor (30%) at global scale, whereas its importance is lower than 10% for boreal and tropical regions (Fig. 3). These patterns may be because thermal limitation to growth at treelines during the summer is most critical in the cold boreal regions, while in the tropics where temperature is high throughout the year, temperature of the wettest season plays a key role in limiting tree growth at treelines. Our results confirm the importance of temperature during the warm part of the year in the boreal zone (Jobbágy & Jackson, 2000), but suggest that precipitation is more important than temperature in temperate regions. It agrees with climatic sensitivity of tree

298 growth in the Norther Hemisphere (Gao et al., 2022). Especially under dry environmental
299 conditions, moisture availability is crucial to limiting tree growth in the treeline ecotone (Liang et
300 al., 2014; Ren et al., 2018).
301
302 Our study provides vastly more data points for each treeline compared to previous global
303 assessments (Jobbágy & Jackson, 2000; Körner & Paulsen, 2004), allowing us to explore for the
304 first time what controls treeline position at a local scale. We found that temperature remains the
305 dominant explanation for the altitudinal variation of 76% of the treeline within a single treeline
306 loop with similar climatic conditions (Fig. S9).
307
308 **3.3. Shifts in closed-loop mountain treelines**
309 Between 2000 and 2010, mountain treelines have shifted upwards at 777 out of the 1,110 treeline
310 loops (70%) and downward at 333 treeline loops (Fig. 4a). The mean global treeline shift rate was
311 an upward shift of 1.2 m/year, which is consistent with case studies of treeline change, with rates >1
312 m/year reported in the literature (Table S2). A synthesis of treeline shift rates reported in the
313 literature suggests the rate was 0.67 m/year before 1970 compared to 4.36 m/year after 1970 and
314 6.16 m/year after 2000 (Fig. S10; Table S2). This provides evidence that the rate of change in
315 treeline elevation is accelerating, possibly due to recent rapid climate change (Bolton et al., 2018).
316 Treeline shift rates in the tropics (mean of 3.1 m/year) were higher than those in boreal and
317 temperate regions (Fig. 4b). The faster changes in the topics could be related to hydrothermal
318 conditions: in the tropics, higher temperature and more abundant precipitation bring a longer
319 growing season, which naturally favours the growth of seedlings and young trees. By contrast, there
320 is a slight downward shift in temperate regions (an average of -0.5 m/year), where the position of
321 the treeline is dominated by precipitation (Fig. 3c). This could be due to decreasing precipitation
322 in some mountain areas of the temperate zone, for example in northern China (Piao et al., 2010).
323

Although the tropical CLMT have the fastest shift rates, their variability is the largest, ranging from -10.2 to 16.9 m/year (Fig. 4b). In the tropics, treeline shift rates greater than 10 m/year in the mountains of Malawi, Papua New Guinea, and Indonesia may reflect a more extreme trend in these tropical systems. In other regions, there are also some treelines that have shifted much more than expected (>10 m/year; Fig. 4b): in boreal regions, these expectations are mainly in Russia and Canada; in temperate regions, they are geographically concentrated in East Asia (North Korea, Japan, and China). On the contrary, there are also cases of treelines receding at a high rate, possibly driven by fire in some areas, either through the physical destruction of trees that acts to lower the existing treelines, or through the destruction of seedlings established upslope that acts to prevent treeline advances (Kim & Lee, 2015). For example, treelines have significantly receded in the western USA where climate and vegetation are favourable for fire (Seven Devils Mountains, Swan Range, etc.; Fig. 4a).

In addition, independent analysis for the changes in annual maximum Normalized Difference Vegetation Index (NDVI) at CLMT that we identified for the year 2000 shows the NDVI has significantly increased by 3.3% by 2020, at a rate of 0.0012 per year ($P < 0.01$; Fig. S11a). There are significant positive trends in NDVI at treeline zones in boreal, temperate, and tropical regions during 2000-2020 ($P < 0.01$), and tropical areas have the highest rate, approaching 0.0016 per year (Fig. S11b). The increase in NDVI occurred at most treeline zones (~90%; Fig. S11c). This greening at the treeline may also be conducive to upward movement of the treeline in the future.

4. Discussion

4.1. Comparison of treeline datasets before and after considering human footprint

Although we have examined CLMT by manual interpretation to remove anthropogenic treelines, we further conduct a stricter assessment of human pressures to check whether our results would still be impacted by human activity. We used a global Human Footprint dataset (Mu et al., 2022)

and found 83% of our CLMT in wilderness (Human Footprint < 1) or in highly intact areas (Human Footprint <4). We then removed those treelines with human footprint values ≥ 4, re-ran the analysis with the higher human footprint values excluded, and updated all the results above (Figs. S12-S14). By comparing these new results with those using the whole dataset, we found a similar pattern along latitude and longitude gradients (Figs. 2 and S12). The results regarding climate dominants (Figs. 3 and S13) and treeline shift rates (Figs. 4b and S14) were also consistent using either approach. Thus, the additional criterion to further focus our analysis on treelines with no human disturbance does not alter our overall results or conclusions, and further confirms that our CLMT product can well represent the change and pattern of climatic treelines.

4.2. Implications of treeline shifts for carbon, biodiversity, and hydrology

Changing treeline position can affect the carbon cycle, biodiversity, and hydrological processes in mountain environments. Mountain treelines moving upward to higher elevations increase woody biomass at and above the treeline, accumulating carbon and increasing their ability to act as carbon sinks (Lopatin et al., 2006; Tarnocai et al., 2009). However, such increases may be offset by increases in soil respiration, leading to a net loss of ecosystem carbon (Wilmking et al., 2006; Hartley et al., 2012). The ascent of mountain treelines also substantially influences biodiversity patterns at high elevations, with enhanced habitat loss of endemic alpine species within a narrow range of mountains (Wang et al., 2022) and potential expansion of habitat for forest-dependent species whose upper range limits coincide with the treeline ecotones (Elsen et al., 2017). For alpine species isolated at the top of mountains, upward treeline shifts could increase the risk of extinction, where there is not enough room for the alpine zone to move upward under future climate change (Dirnböck et al., 2011). In Siberia, for example, we show many treelines have shifted upwards (Fig. 4b), inevitably reducing the area of the tundra, which is rich in floristic and species diversity and supports indigenous land use types. The expansion of Siberian forests has been predicted to continue, thus causing huge losses of tundra in the future (Kruse & Herzschuh, 2022). While we

focused here on treeline shifts in areas with minimal human impacts, treeline ascent in areas with pronounced human disturbance will further hinder species' ability to track vegetation changes and likely lead to more pronounced population declines (Feeley & Silman, 2010; Elsen et al., 2020). There are many instances with high pressure in high-elevation areas, especially from burning, grazing, and wood harvesting (Bader et al., 2008; Jiménez-García et al., 2021). The combined impact of shifting treelines and human disturbances may also affect local livelihoods and act as a double-blow for sensitive alpine species. In addition, tree expansions into the formerly treeless area may alter downstream water supply. Recent advances of the treeline have decreased the area of alpine tundra, thereby affecting its critical role as a reservoir of freshwater resources and in water release (Barredo et al., 2020).

4.3. Uncertainties and caveats

To isolate the impacts of climate on treelines, our analysis identifies CLMT that completely encircle a mountain. However, focusing on this kind of treelines could omit some climate-related treelines as climatic treelines may not be in a closed loop shape in some cases. We acknowledge that our CLMT database does not include all climatic treelines, but is a subset of climatic treelines that specifically form a closed loop, because these enable us to analyse climatic determinants with greater confidence. We also note that tree cover can increase in various ways, either through new or existing trees growing above the 5 m height threshold, or existing trees having increased canopy cover. However, our analysis is based on the definition of treeline according to remotely sensed tree cover, and we used this definition to assess treeline position at two time periods and assess change. While our analysis period is short and errors will exist at a pixel scale, our global detection of a shifting treeline provides an early indication of climate-induced changes that need to be carefully monitored in the future. To reduce uncertainties and further advance our understanding of treeline dynamics, future studies require more high-resolution remote sensing products for a longer period and more field data in alpine treeline zones for cross-validation.

5. Conclusion

Our study develops a novel remote sensing-based algorithm to map closed-loop treelines across global mountain regions, isolating the effects of climate on treeline position. Our approach provides a globally consistent way of detecting and monitoring closed-loop treelines around mountains, which are more likely to reflect natural systems with minimal impact of land-use change. Focusing on these closed-loop treelines as a proxy for natural treelines allows us to isolate the impacts of climate and climate change on the elevation distribution and change of treelines. We found temperature was the dominant control on natural treelines both at a global and local scale. Our results indicated an upward migration of treelines over the period 2000 to 2010 in boreal and tropical regions but a slight downward shift in temperate zones. Our new findings and the global closed-loop mountain treeline database produced in this study also provides a useful tool for biodiversity and carbon assessments, ecological modelling, and analyses of adaptation of species to future climate change.

Acknowledgments

X.H. was funded by a PhD scholarship from Southern University of Science and Technology hosted jointly with the University of Leeds. Z.Z. was supported by the National Natural Science Foundation of China (no. 42071022) and the start-up fund provided by Southern University of Science and Technology (no. 29/Y01296122). We thank Hansen/UMD/Google/USGS/NASA for providing the high-resolution tree cover data; NASA and Japan's Ministry of Economy, Trade and Industry for providing the elevation data; Körner for providing the GMBA inventory; Fick and Hijmans for providing WorldClim data; and Google Earth for providing very-high-resolution satellite imagery.

Author contributions

X.H., Z.Z., D.V.S. and J.H. designed the research; X.H. performed the analysis and wrote the draft; and all the authors contributed to the interpretation of the results and the writing of the paper.

Data availability statement

The global tree cover data in 2000 are available at https://earthenginepartners.appspot.com/science-2013-global-forest/download_v1.7.html and the tree cover data in 2010 are available at https://glad.umd.edu/Potapov/TCC_2010/. The ASTER elevation data are available at https://earthdata.nasa.gov/. The GMBA inventory is available at https://ilias.unibe.ch/goto_ilias3_unibe_cat_1000515.html. The WorldClim climate data are available at https://www.worldclim.org/data/worldclim21.html. The MODIS combined 16-day NDVI is available at https://developers.google.com/earth-engine/datasets/catalog/MODIS_MCD43A4_006_NDVI. The scripts used to generate the results/figures are available in GitHub at https://github.com/hexinyue33/treeline. The global closed-loop mountain treeline (CLMT) database developed in this study can be accessed through https://hexinyue33.users.earthengine.app/view/clmt.

References

Ameztegui, A., Coll, L., Brotons, L., & Ninot, J.M. (2016). Land-use legacies rather than climate change are driving the recent upward shift of the mountain tree line in the P yrenees. Global Ecology and Biogeography, 25(3), 263-273. https://doi.org/10.1111/geb.12407

Bader, M.Y., Rietkerk, M., & Bregt, A.K. (2008). A simple spatial model exploring positive feedbacks at tropical alpine treelines. Arctic, Antarctic, and Alpine Research, 40(2), 269-278. https://doi.org/10.1657/1523-0430(07-024)[BADER]2.0.CO;2

Barredo, J. I., Mauri, A., & Caudullo, G. (2020). Alpine tundra contraction under future warming scenarios in Europe. Atmosphere, 11(7), 698. https://doi.org/10.3390/atmos11070698

Birre, D., Feuillet, T., Lagalis, R., Milian, J., Alexandre, F., Sheeren, D., Serrano-Notivoli, R., Vignal, M., & Bader, M.Y., (2023). A new method for quantifying treeline-ecotone change based on multiple spatial pattern dimensions. Landscape Ecology, 1-18. https://doi.org/10.1007/s10980-022-01589-4

Bolton, D.K., Coops, N.C., Hermosilla, T., Wulder, M.A., & White, J.C. (2018). Evidence of vegetation greening at alpine treeline ecotones: three decades of Landsat spectral trends informed by lidar-derived vertical structure. Environmental Research Letters, 13(8), 084022. https://doi.org/10.1088/1748-9326/aad5d2

Camarero, J.J., Gazol, A., Sánchez-Salguero, R., Fajardo, A., McIntire E J B, Gutiérrez E, Batllori E, Boudreau S, Carrer M, Diez J, Dufour-Tremblay G, Gaire NP, Hofgaard A, Jomelli V, Kirdyanov AV, Lévesque E, Liang E, Linares JC, Mathisen IE, Moiseev PA, Sangüesa-Barreda G, Shrestha KB, Toivonen JM , Tutubalina OV, & Wilmking M. (2021). Global fading of the temperature-growth coupling at alpine and polar treelines. Global Change Biology, 27(9), 1879-1889. https://doi.org/10.1111/gcb.15530

Cieraad, E., McGlone, M. S., & Huntley, B. (2014). Southern Hemisphere temperate tree lines are not climatically depressed. Journal of Biogeography, 41(8), 1456-1466. https://doi.org/10.1111/jbi.12308

469 Dirnböck, T., Essl, F., & Rabitsch, W. (2011). Disproportional risk for habitat loss of high-altitude
470 endemic species under climate change. Global Change Biology, 17(2), 990-996.
471 https://doi.org/10.1111/j.1365-2486.2010.02266.x
472 Du, H., Liu, J., Li, M.-H., Büntgen, U., Yang, Y., Wang, L., Wu, Z., & He, H.S. (2018). Warming-
473 induced upward migration of the alpine treeline in the Changbai Mountains, northeast China.
474 Global Change Biology, 24(3), 1256-1266. https://doi.org/10.1111/gcb.13963
475 Elliott, G.P., & Cowell, C.M. (2015). Slope aspect mediates fine-scale tree establishment patterns
476 at upper treeline during wet and dry periods of the 20th century. Arctic, Antarctic, and Alpine
477 Research, 47(4), 681-692. https://doi.org/10.1657/AAAR0014-025
478 Elsen, P. R., Tingley, M. W., Kalyanaraman, R., Ramesh, K., & Wilcove, D. S. (2017). The role
479 of competition, ecotones, and temperature in the elevational distribution of Himalayan birds.
480 Ecology, 98(2), 337-348. https://doi.org/10.1002/ecy.1669
481 Elsen, P. R., Monahan, W. B., & Merenlender, A. M. (2020). Topography and human pressure in
482 mountain ranges alter expected species responses to climate change. Nature Communications,
483 11(1), 1-10. https://doi.org/10.1038/s41467-020-15881-x
484 Feeley, K. J., & Silman, M. R. (2010). Land-use and climate change effects on population size and
485 extinction risk of Andean plants. Global Change Biology, 16(12), 3215-3222.
486 https://doi.org/10.1111/j.1365-2486.2010.02197.x
487 Fick, S.E., & Hijmans, R.J. (2017). WorldClim 2: new 1-km spatial resolution climate surfaces for
488 global land areas. International Journal of Climatology, 37(12), 4302-4315.
489 https://doi.org/10.1002/joc.5086
490 Friedman, J.H. (2001). Greedy function approximation: a gradient boosting machine. Annals of
491 Statistics, 29, 1189-1232.
492 Gao, S., Liang, E., Liu, R., Babst, F., Camarero, J.J., Fu, Y.H., Piao, S., Rossi, S., Shen, M., Wang,
493 T., & Peñuelas, J. (2022). An earlier start of the thermal growing season enhances tree growth

494 in cold humid areas but not in dry areas. Nature Ecology & Evolution, 6(4), 397-404.
495 https://doi.org/10.1038/s41559-022-01668-4
496 Gehrig-Fasel, J., Guisan, A., & Zimmermann, N.E. (2007). Tree line shifts in the Swiss Alps:
497 Climate change or land abandonment? Journal of Vegetation Science, 18, 571-582.
498 https://doi.org/10.1111/j.1654-1103.2007.tb02571.x
499 Grace, J. (1989). Tree lines. Philosophical Transactions of the Royal Society of London. B,
500 Biological Sciences, 324(1223), 233-245.
501 Hansen, M.C., Potapov, P.V., Moore, R., Hancher, M., Turubanova, S.A., Tyukavina, A., Thau,
502 D., Stehman, S.V., Goetz, S.J., & Loveland, T.R. (2013). High-resolution global maps of 21st-
503 century forest cover change. Science, 342(6160), 850-853.
504 https://doi.org/10.1126/science.1244693
505 Harsch, M. A., Hulme, P. E., McGlone, M. S., & Duncan, R. P. (2009). Are treelines advancing?
506 A global meta-analysis of treeline response to climate warming. Ecology Letters, 12(10),
507 1040-1049. https://doi.org/10.1111/j.1461-0248.2009.01355.x
508 Hartley, I.P., Garnett, M.H., Sommerkorn, M., Hopkins, D.W., Fletcher, B.J., Sloan, V. L.,
509 Phoenix, G.K., & Wookey, P.A. (2012). A potential loss of carbon associated with greater
510 plant growth in the European Arctic. Nature Climate Change, 2(12), 875-879.
511 https://doi.org/10.1038/nclimate1575
512 Holtmeier, F. & Broll, G. (2005). Sensitivity and response of northern hemisphere altitudinal and
513 polar treelines to environmental change at landscape and local scales. Global Ecology
514 Biogeography, 14(5), 395-410. https://doi.org/10.1111/j.1466-822X.2005.00168.x
515 Irl, S.D., Anthelme, F., Harter, D.E., Jentsch, A., Lotter, E., Steinbauer, M.J., & Beierkuhnlein, C.
516 (2016). Patterns of island treeline elevation–a global perspective. Ecography, 39(5), 427-436.
517 https://doi.org/10.1111/ecog.01266

518 Jiménez-García, D., Li, X., Lira-Noriega, A., & Peterson, A.T. (2021). Upward shifts in elevational
519 limits of forest and grassland for Mexican volcanoes over three decades. Biotropica, 53, 798-
520 807. https://doi.org/10.1111/btp.12942
521 Jobbágy, E.G. & Jackson, R.B. (2000). Global controls of forest line elevation in the northern and
522 southern hemispheres. Global Ecology Biogeography, 9(3), 253-268.
523 https://doi.org/10.1046/j.1365-2699.2000.00162.x
524 Karger, D.N., Kessler, M., Conrad, O., Weigelt, P., Kreft, H., König, C., & Zimmermann, N.E.
525 (2019). Why tree lines are lower on islands—Climatic and biogeographic effects hold the
526 answer. Global Ecology Biogeography, 28(6), 839-850. https://doi.org/10.1111/geb.12897
527 Ke, G., Meng, Q., Finley, T., Wang, T., Chen, W., Ma, W., Ye, Q., & Liu, T.-Y. (2017). Lightgbm:
528 A highly efficient gradient boosting decision tree. Advances in Neural Information Processing
529 Systems, 30, 3146-3154.
530 Kim, J.W., & Lee, J.S. (2015). Dynamics of alpine treelines: positive feedbacks and global,
531 regional and local controls. Journal of Ecology and Environment, 38(1), 1-14.
532 https://doi.org/10.5141/ecoenv.2015.001
533 Körner, C. & Paulsen, J. (2004). A world-wide study of high altitude treeline temperatures. Journal
534 of Biogeography, 31(5), 713-732. https://doi.org/10.1111/j.1365-2699.2003.01043.x
535 Körner, C., Jetz, W., Paulsen, J., Payne, D., Rudmann-Maurer, K., & M. Spehn, E. (2017). A global
536 inventory of mountains for bio-geographical applications. Alpine Botany, 127(1), 1-15.
537 https://doi.org/10.1007/s00035-016-0182-6
538 Kruse, S., & Herzschuh, U. (2022). Regional opportunities for tundra conservation in the next 1000
539 years. eLife, 11, e75163. https://doi.org/10.7554/eLife.75163
540 Liang, E., Dawadi, B., Pederson, N., & Eckstein, D. (2014). Is the growth of birch at the upper
541 timberline in the Himalayas limited by moisture or by temperature? Ecology, 95(9), 2453-
542 2465. https://doi.org/10.1890/13-1904.1

Lyu, L., Zhang, Q.B., Pellatt, M.G., Büntgen, U., Li, M.H., & Cherubini, P. (2019). Drought limitation on tree growth at the Northern Hemisphere's highest tree line. Dendrochronologia, 53, 40-47. https://doi.org/10.1016/j.dendro.2018.11.006

Lopatin, E., Kolström, T., & Spiecker, H. (2006). Determination of forest growth trends in Komi Republic (northwestern Russia): combination of tree-ring analysis and remote sensing data. Boreal Environment Research, 11, 341-353.

Lu, X., Liang, E., Wang, Y., Babst, F., & Camarero, J.J. (2021). Mountain treelines climb slowly despite rapid climate warming. Global Ecology and Biogeography, 30(1), 305-315. https://doi.org/10.1111/geb.13214

Mohapatra, J., Singh, C.P., Tripathi, O.P., & Pandya, H.A. (2019). Remote sensing of alpine treeline ecotone dynamics and phenology in Arunachal Pradesh Himalaya. International Journal of Remote Sensing, 40(20), 7986-8009. https://doi.org/10.1080/01431161.2019.1608383

Mu, H., Li, X., Wen, Y., Huang, J., Du, P., Su, W., Miao, S., & Geng, M. (2022). A global record of annual terrestrial Human Footprint dataset from 2000 to 2018. Scientific Data, 9(1), 176. https://doi.org/10.1038/s41597-022-01284-8

Paulsen, J. & Körner, C. (2014) A climate-based model to predict potential treeline position around the globe. Alpine Botany, 124(1), 1-12. https://doi.org/10.1007/s00035-014-0124-0

Potapov, P., Turubanova, S., Tyukavina, A., Krylov, A., McCarty, J., Radeloff, V., & Hansen, M. (2015). Eastern Europe's forest cover dynamics from 1985 to 2012 quantified from the full Landsat archive: Remote Sensing of Environment, 159, 28-43. https://doi.org/10.1016/j.rse.2014.11.027

Piao, S., Ciais, P., Huang, Y., Shen, Z., Peng, S., Li, J., Zhou, L., Liu, H., Ma, Y., Ding, Y. and Friedlingstein, P. (2010). The impacts of climate change on water resources and agriculture in China. Nature, 467(7311), 43-51. https://doi.org/10.1038/nature09364

568 Ren, P., Rossi, S., Camarero, J.J., Ellison, A.M., Liang, E., & Peñuelas, J. (2018). Critical
569 temperature and precipitation thresholds for the onset of xylogenesis of Juniperus przewalskii
570 in a semi-arid area of the north-eastern Tibetan Plateau. Annals of Botany, 121(4), 617-624.
571 https://doi.org/10.1093/aob/mcx188
572 Sigdel, S.R., Wang, Y., Camarero, J.J., Zhu, H., Liang, E., & Peñuelas, J. (2018). Moisture-
573 mediated responsiveness of treeline shifts to global warming in the Himalayas. Global Change
574 Biology, 24(11), 5549-5559. https://doi.org/10.1111/gcb.14428
575 Tachikawa, T., Hato, M., Kaku, M., & Iwasaki, A. (2011). Characteristics of ASTER GDEM
576 version 2. In: 2011 IEEE International Geoscience and Remote Sensing Symposium: IEEE,
577 3657-3660. https://doi.org/10.1109/IGARSS.2011.6050017
578 Tarnocai, C., Canadell, J.G., Schuur, E.A.G., Kuhry, P., Mazhitova, G., & Zimov, S. (2009). Soil
579 organic carbon pools in the northern circumpolar permafrost region. Global Biogeochemical
580 Cycles, 23, GB2023. https://doi.org/10.1029/2008GB003327
581 Testolin, R., Attorre, F., & Jiménez-Alfaro, B. (2020). Global distribution and bioclimatic
582 characterization of alpine biomes. Ecography, 43(6), 779-788.
583 https://doi.org/10.1111/ecog.05012
584 Verrall, B. & Pickering, C.M. (2020). Alpine vegetation in the context of climate change: A global
585 review of past research and future directions. Science of the Total Environment, 748, 141344.
586 https://doi.org/10.1016/j.scitotenv.2020.141344
587 Wang, X., Wang, T., Xu, J., Shen, Z., Yang, Y., Chen, A., Wang, S., Liang, E., & Piao, S. (2022).
588 Enhanced habitat loss of the Himalayan endemic flora driven by warming-forced upslope tree
589 expansion. Nature Ecology & Evolution, 6(7), 890-899. https://doi.org/10.1038/s41559-022-
590 01774-3
591 Wardle, P. & Coleman, M. (1992). Evidence for rising upper limits of four native New Zealand
592 forest trees. New Zealand Journal of Botany, 30(3), 303-314.
593 https://doi.org/10.1080/0028825X.1992.10412909

Wei, C., Karger, D.N., & Wilson, A.M. Spatial detection of alpine treeline ecotones in the Western United States. Remote Sensing of Environment, 2020, 240, 111672. https://doi.org/10.1016/j.rse.2020.111672

Wilmking, M., Harden, J., & Tape, K. (2006). Effect of tree line advance on carbon storage in NW Alaska. Journal of Geophysical Research, 111, 1-10. https://doi.org/10.1029/2005JG000074

Xu, D., Geng, Q., Jin, C., Xu, Z., & Xu, X. (2020). Tree Line Identification and Dynamics under Climate Change in Wuyishan National Park Based on Landsat Images. Remote Sensing, 12(18), 2890. https://doi.org/10.3390/rs12182890

603 **Figure Legends**

604 **Figure 1. Global distribution of closed-loop mountain treeline (CLMT) elevation.** To improve
605 readability, plot **(a)** is based on the mean value of each closed-loop mountain treeline (at each 30-
606 m pixel). Grey boundaries indicate mountain regions defined by GMBA inventory data. **(b)**–**(g)**
607 show examples of CLMT extraction results superimposed with Google Earth images. The yellow
608 line represents the position of the treeline, and the green circle shows the highest elevation point
609 that formed the starting point of each search by the treeline algorithm.
610
611 **Figure 2. Global latitudinal (a) and longitudinal (b) variation of closed-loop mountain treeline**
612 **(CLMT) elevation.** Different symbols represent different regions and colours represent the
613 distance to the coast. The data points show the mean elevation of all of the pixels in the CLMT.
614 The error bar is the elevation range of the corresponding treeline loop.
615
616 **Figure 3. Climate drivers controlling the variability in treeline elevation for the globe (a),**
617 **boreal (≥50°N, b), temperate (23.5° – 50°N/S, c) and tropical (23.5°N – 23.5°S, d) regions.**
618
619 **Figure 4. Closed-loop mountain treeline (CLMT) shift rate during 2000-2010. (a)**, Spatial
620 pattern of CLMT shift rate. **(b)**, Box-plot showing CLMT shift rate in boreal (≥50°N), temperate
621 (23.5° – 50°N/S) and tropical (23.5°N – 23.5°S) regions (central line: median; red dot: mean; box:
622 25^{th} and 75^{th} percentiles, respectively; error bar: maximum and minimum whisker values; +:
623 maximum and minimum values). The black dashed line is the zero line. Numbers of the studied
624 CLMT are shown above the boxes.
625

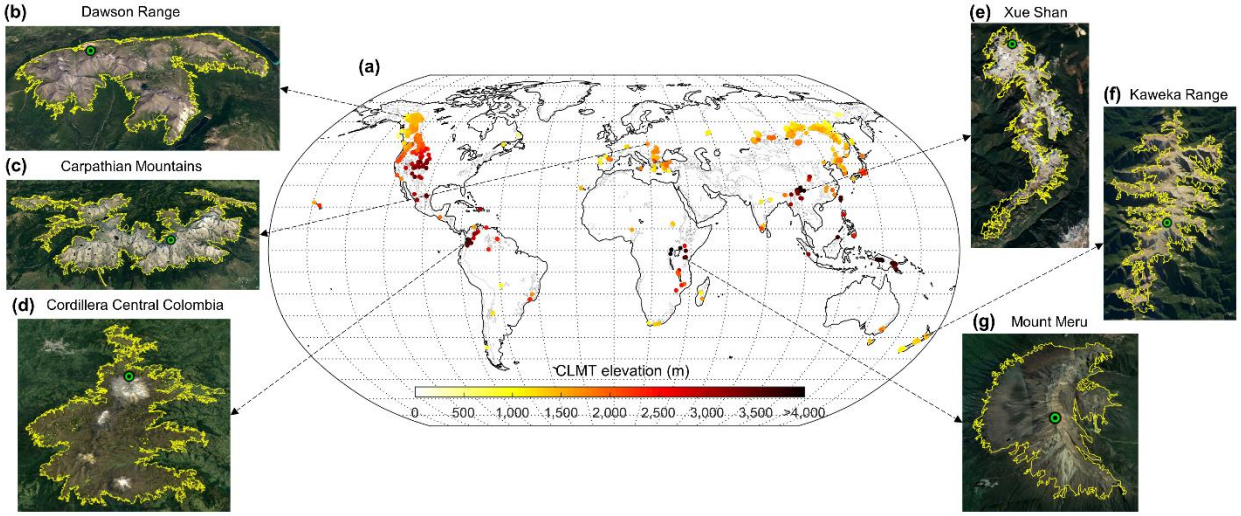

626

627 **Figure 1. Global distribution of closed-loop mountain treeline (CLMT) elevation.** To improve
628 readability, plot **(a)** is based on the mean value of each closed-loop mountain treeline (at each 30-
629 m pixel). Grey boundaries indicate mountain regions defined by GMBA inventory data. **(b)**–**(g)**
630 show examples of CLMT extraction results superimposed with Google Earth images. The yellow
631 line represents the position of the treeline, and the green circle shows the highest elevation point
632 that formed the starting point of each search by the treeline algorithm.

633

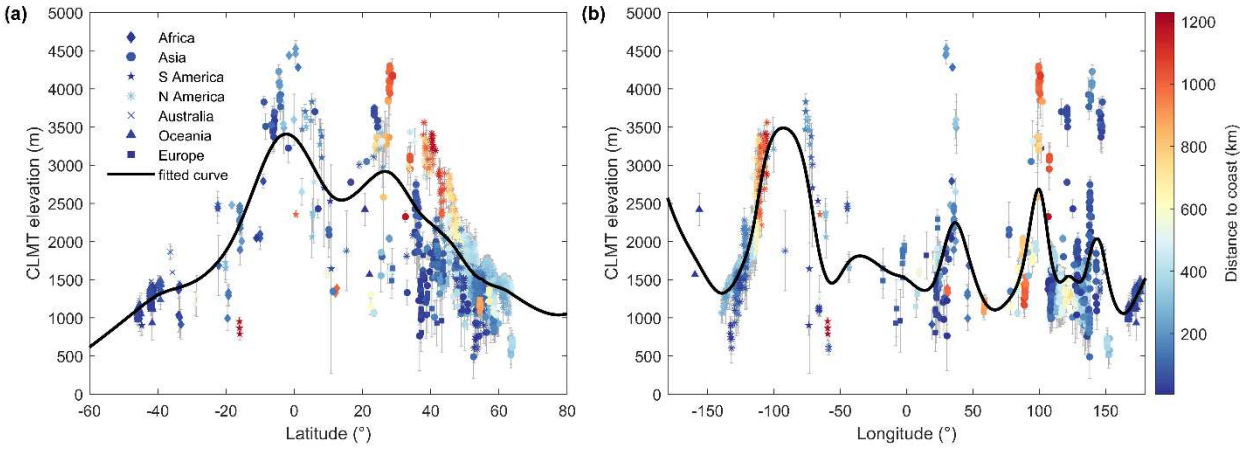

634

635 **Figure 2. Global latitudinal (a) and longitudinal (b) variation of closed-loop mountain treeline**
636 **(CLMT) elevation.** Different symbols represent different regions and colours represent the
637 distance to the coast. The data points show the mean elevation of all of the pixels in the CLMT.
638 The error bar is the elevation range of the corresponding treeline loop.

639

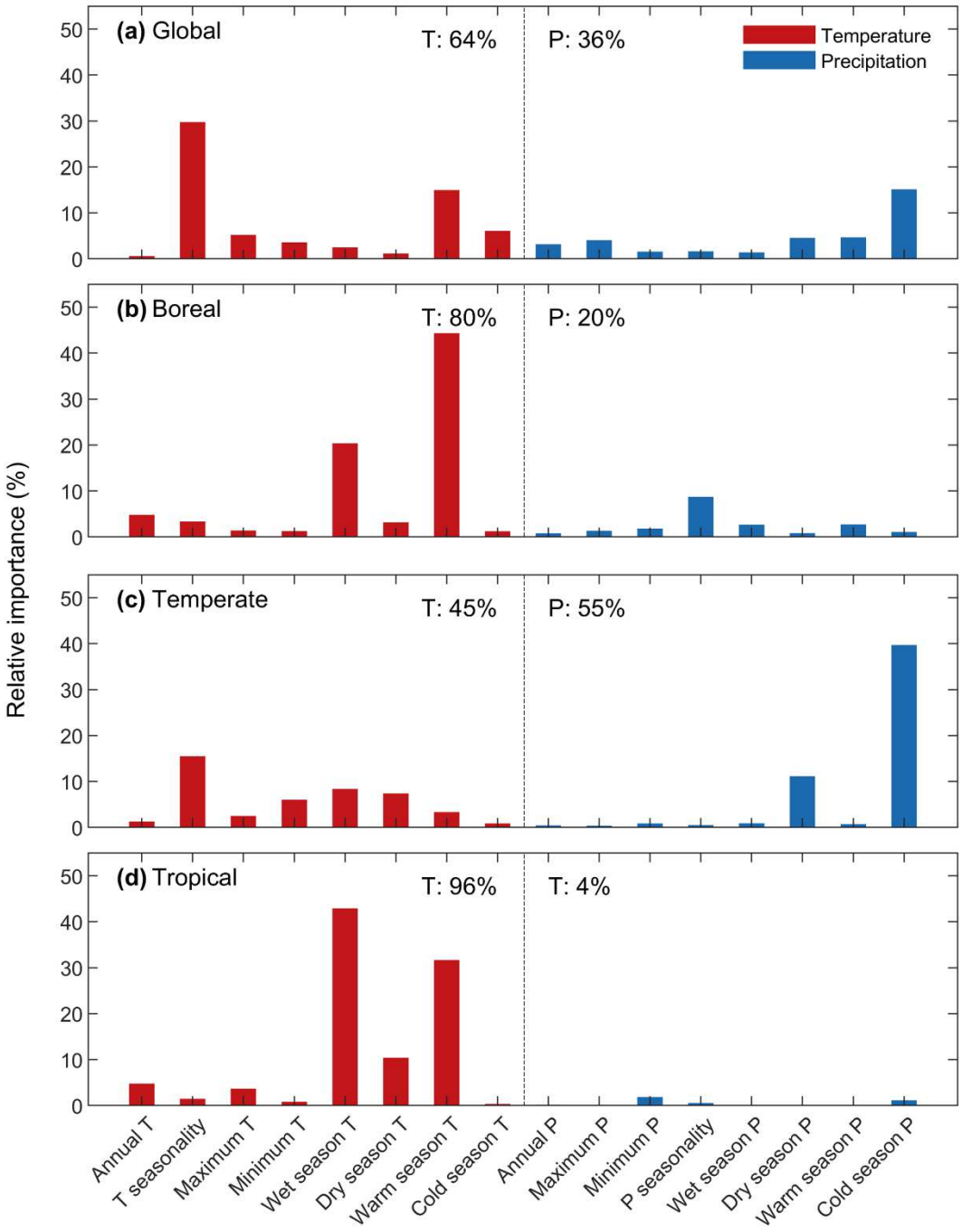

640

641 **Figure 3. Climate drivers controlling the variability in treeline elevation for the globe (a),**

642 **boreal (≥50°N, b), temperate (23.5° – 50°N/S, c) and tropical (23.5°N – 23.5°S, d) regions.**

643

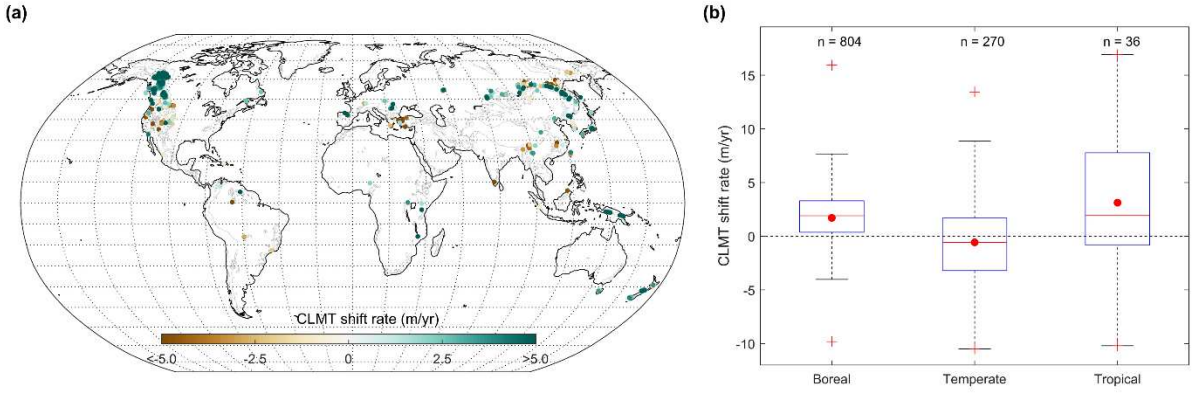

644

645 **Figure 4. Closed-loop mountain treeline (CLMT) shift rate during 2000-2010. (a)**, Spatial
646 pattern of CLMT shift rate. **(b)**, Box-plot showing CLMT shift rate in boreal (≥50°N), temperate
647 (23.5° – 50°N/S) and tropical (23.5°N – 23.5°S) regions (central line: median; red dot: mean; box:
648 25th and 75th percentiles, respectively; error bar: maximum and minimum whisker values; +:
649 maximum and minimum values). The black dashed line is the zero line. Numbers of the studied
650 CLMT are shown above the boxes.